ACS Photonics

Article

pubs.acs.org/journal/apchd5

Fast and Transparent Adaptive Lens Based on Plasmonic Heating

Jon S. Donner,[†] Jordi Morales-Dalmau,[†] Irene Alda,[†] Renaud Marty,[†] and Romain Quidant*[,†,‡]

[†]ICFO- The Institute of Photonic Sciences, Mediterranean Technology Park, 08860, Castelldefels (Barcelona), Spain

[‡]ICREA – Institució Catalana de Recerca i Estudis Avançats, 08010 Barcelona, Spain

Supporting Information

ABSTRACT: In the current trend toward miniaturization, integrated micro-optical elements play a central role in the development of various applications including high-density data storage and imaging. In these operations, fine alignment and focus adjustment are usually performed mechanically, thus, limiting the accuracy, size and speed of devices. Here, we propose a novel reconfigurable microlens based on the engineering of the temperature distribution induced by a patterned plasmonic surface shined with a resonant near-infrared light. The refractive index change generated in a surrounding thermo-optical material acts as an effective lens whose parameters are remotely adjusted by the control near-infrared light. We demonstrate focal distance tunability of tens of microns with subnanometer accuracy along with time-responses down to 200 μs. The applicability of this photothermal lens is proved in the framework of optical microscopy and adaptive optics.

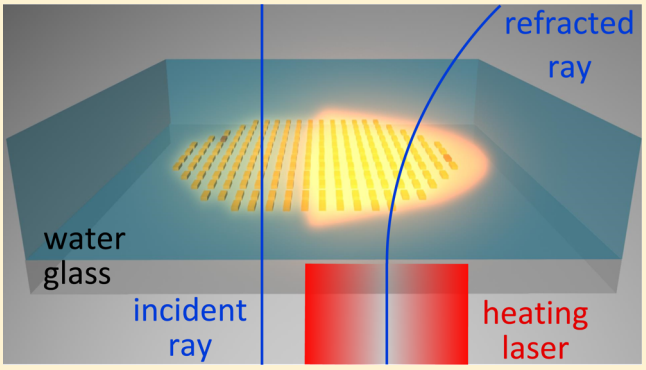

KEYWORDS: *micro-optical devices, lenses, adaptive imaging, active imaging, 3D microscopy, thermoplasmonics*

Adaptive optical elements that enable dynamic control of optical paths are important components of the last generation of commercial optical devices.[1−16] In this context, various approaches of reconfigurable optical microlenses based on shaping the surface of a liquid drop with pH-tunable hydrogels,[10,17,18] pressure regulation of polymer surfaces,[11−13,15,16] and refractive-index-adjustable liquid crystals[19,20] were developed. Although such strategies imply some constraints for integration into complex devices, they have shown to be a powerful way to adjust the focus with time responses ranging from seconds to few milliseconds.[10−12,15,16,21] Another widely used reconfigurable element is the Spatial Light Modulator (SLM).[22,23] SLMs, typically based on liquid crystals technology, offer a great control over light beams but they are limited to operation in reflection mode with time responses between 10−100 ms. Other major disadvantages are their bulkiness and price. Finally, one of the most competitive technologies is the deformable mirror, whose surface can be dynamically deformed using miniaturized actuators. With a time response of the order of 100 μs, this technology has greatly contributed to the field of adaptive optics with applications especially in astronomy, microscopy, and beaming technology. However, they are by definition limited to reflection mode and this is a crucial roadblock in many applications. In this letter, we introduce a novel concept that enables us to transform any conventional (static) optical lens into an effective Adaptive Photo-Thermal (APT) lens whose image focal plane can be dynamically shaped by a control optical signal. Our approach relies on the temperature-dependence of the refractive index of matter. A local increase of temperature induces a gradient of refractive index that affects the propagation of optical rays. In the early 2000s it was proposed to exploit this effect for the detection of single absorbing nano-objects.[24,25] In such two color experiments, one laser is used to heat up the nano-object, while the second probes the associated local change of refractive index. This has enabled researchers to accurately locate and dynamically track single metallic nanoparticles[24] and carbon nanotubes,[26] as well as single molecules.[25] In parallel, recent advances in so-called thermoplasmonics have led to an unprecedented control of temperature at the micro- and nanoscale.[27,28] Noble metal nanostructures, supporting localized surface plasmons, can be designed to act as efficient punctual heat sources remotely operated by light. Beyond enabling strong temperature gradients at the nanometer scale,[29,30] this method also benefits from very fast heating/cooling dynamics.[27,30] The incentive behind the present work is to exploit such control to engineer a temperature landscape that can locally modify the focal plane of a conventional optical lens and ultimately transform it into an adaptive imaging element.

RESULTS AND METHODS

In the implementation presented here (sketched in Figure 1), the surface of a glass coverslip is patterned with plasmonic

Received: October 24, 2014
Published: January 29, 2015

DOI: 10.1021/ph500392c
ACS Photonics 2015, 2, 355−360

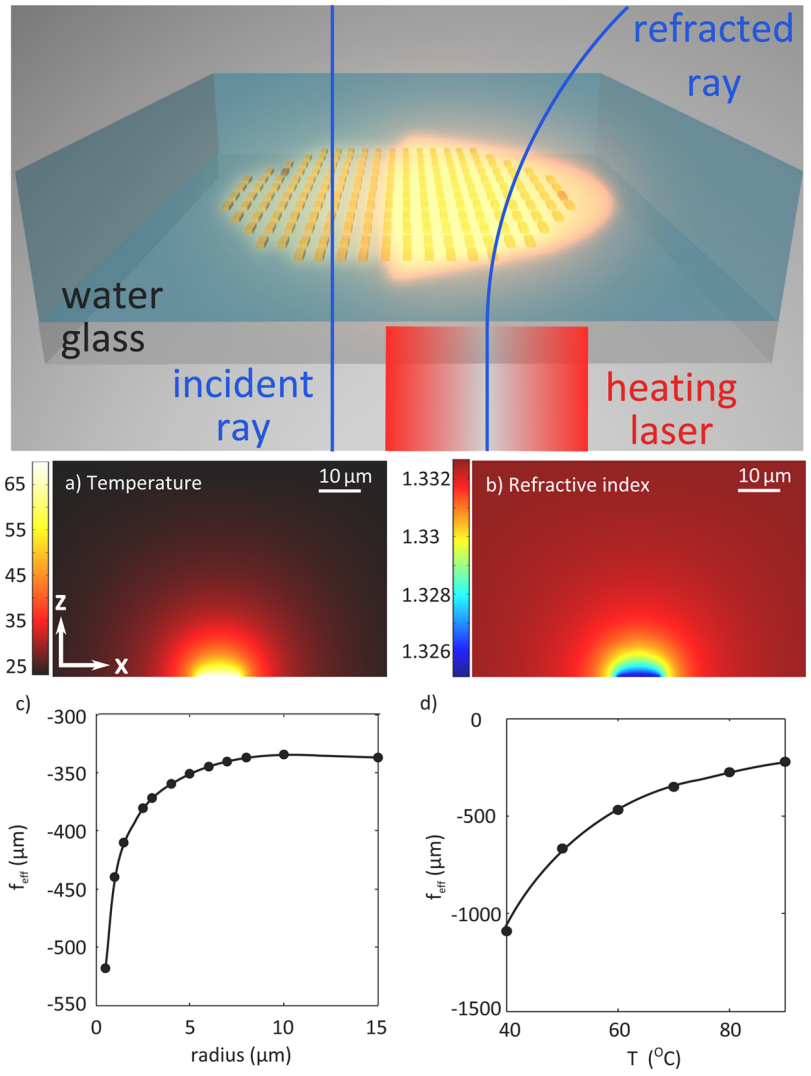

Figure 1. Principle of the APT lens: In the presence of a heating laser (red beam), the temperature in the vicinity of an array of absorbing nanostructures is increased. The resulting profile of refractive index refracts a collimated blue light beam propagating along the *Z*-axis. (a) Temperature map around a 5 μm radius gold disk heated to 70 °C and submerged in water (cut in *XZ* plane). (b) Associated refractive index map calculated for a wavelength of 473 nm to match the wavelength used in the experiment. (c, d) Evolution of the effective focal distance f_{eff} with the disk size while maintaining a fixed temperature (T = 70 °C in (c)) and with the temperature of the disk for a fixed radius (r = 5 μm in (d)).

nanostructures that create, upon resonant illumination, the desired distribution of temperature.[28] On top of the patterned surface is placed a 100 μm thick chamber filled with water that acts as the index-changing thermo-optical medium.[31] Alternatively, other thermo-optical materials with significant $\Delta n/\Delta T$ can be used instead of water.

In order to comprehend the properties of the APT lens, we first simulate the optical lensing effect induced by a micrometer sized heat source. We calculate the temperature profile induced by a 5 μm homogeneous gold pad heated to 70 °C, lying on a glass substrate, and immersed in water (Figure 1a). Because of the cylindrical symmetry, the configuration is fully defined by a slice across the *XZ* plane. Using the temperature-dependent optical index of water,[31] we obtain the profile of the optical index, as shown in Figure 1b. The refractive index of water decreases with increasing temperature and, thus, features a minimum at the center of the heat source. Such a gradient leads to a negative phase accumulation for light propagating through the thermo optical material, which is associated with a divergent lens. By integrating the refractive index variation along the *Z*-direction and using the paraxial approximation we define the effective focal distance f_{eff} of the APT lens as well as its thickness and in-plane profile (see section 1 of the Supporting Information). Figure 1c,d shows the evolution of f_{eff} as a function of the disk diameter and temperature. The lensing power increases with the disk size before saturating for radii larger than 8 μm. A 5 μm radius heat source appears to be a good compromise between lensing ability and compactness. Once identified the optimum size for the heating structure, we show in Figure 1d that temperature variation of the structure enables tuning f_{eff} over a wide range. Indeed, a temperature increase from 40 °C to 90 °C leads to a decrease of the focal distance from −1100 to −220 μm, respectively. This is particularly interesting since it allows dynamic tuning of the lensing effect only by changing the intensity of the heating laser.

Based on these simulations, we have performed a first set of experiments to demonstrate the feasibility of the APT lens concept and assess its performance. To create the desired distribution of temperature,[28] we exploit the capability of plasmonic nanoparticles to efficiently generate heat[27,29,32] when

DOI: 10.1021/ph500392c
ACS Photonics 2015, 2, 355−360

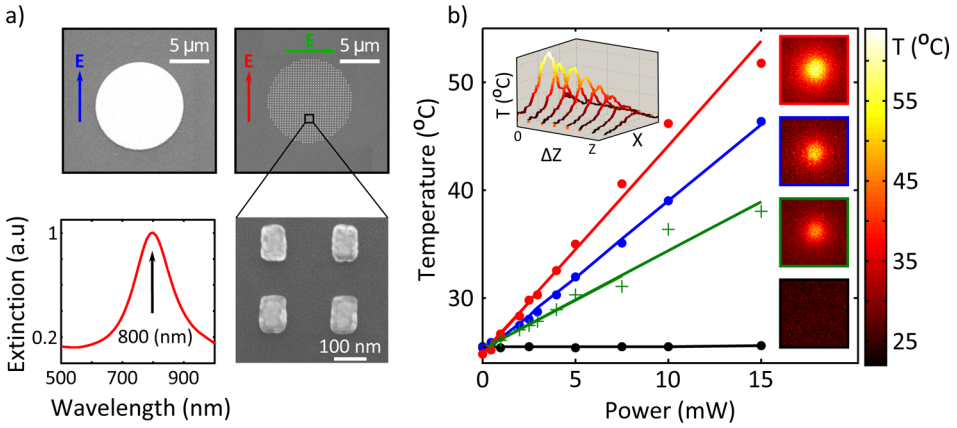

Figure 2. Experimental monitoring of the photothermal properties of APT lenses. (a) SEM images of a homogeneous 5 μm radius gold disk (left) and a 5 μm radius disk made of gold nanorods (right). A higher magnification image of the 120 × 80 × 50 nm^3 nanorods is presented (bottom right) along with their corresponding extinction spectrum displaying a plasmonic resonance in the NIR at 800 nm (bottom left). The NRs spectrum was measured on a square array (30 × 30 μm^2 and 300 nm pitch) using a commercial Andor Shamrock 303i spectrometer attached to an Olympus BX51 microscope. Both structures were fabricated using standard electron beam lithography, followed by evaporation of an adhesion layer of 2 nm titanium and a layer of 50 nm of gold and, finally, a standard lift-off procedure. (b) Evolution of the induced temperature with the power delivered by a 800 nm laser shined on a NR disk excited at the SPR with a parallel polarization (red dots), the same NR disk excited off resonance using a perpendicular polarized configuration (green crosses), a full gold disk (blue dots), and in absence of any structure (black dots). Associated temperature maps of the different configurations are presented for a heating laser power of 15 mW (insets on the right side). The top left inset shows the evolution of the temperature profile as a function of the height above the NR disk excited with a 800 nm parallel polarized laser beam.

illuminated at their plasmonic resonance. The heat source is formed by a finite periodic array (pitch = 300 nm) of gold nanorods (NR) (120 × 80 × 50 nm^3) that lead to a maximum of absorption in the NIR (Figure 2a), at their longitudinal plasmon resonance, that is, for the incident field linearly polarized along the nanorods long axis.

First, the photothermal properties of the fabricated plasmonic NR patterns are assessed using thermal microscopy based on measuring the Fluorescence Polarization Anisotropy (FPA) of fluorescein in a water/glycerol mixture.[33] Figure 2b shows the linear dependence between the maximum reached temperature and the power of the 800 nm CW heating laser.

By rotating the linear polarization of the heating laser by 90 °C, the temperature decreases by half (green curve), which gives a good approximation of the actual contribution of the NR plasmon resonance to heat generation. Noteworthy, the full disk presents a similar temperature map to the resonant NR disk but the latter enables not only a larger increase of temperature for a given power but also a higher transparency for wavelengths out of the NR resonance peak. Furthermore, the NR disk offers an additional degree of freedom in the control of the heating via polarization. Interestingly, the diffusion of the temperature into the water annihilates the anisotropic shape of the nano-objects themselves, because they are smaller than the diffusion length of temperature in water (see Supporting Information, section 3). Finally, we verify that, for the same power of the heating laser, no significant increase of temperature is measured in the absence of any heating structure (black curve).

Subsequently, to observe and characterize the APT lensing effect, we design a simple experiment (depicted in Figure 3a) in which we monitor the changes in the focus of a blue laser diode (λ = 473 nm) propagating through the APT lens. To do so, a NR gold disk is sealed in a thin chamber filled with water that is placed in the optical path of a microscope, right after a 50× microscope objective, as depicted in Figure 3a. First, we performed an experiment whereby we image the blue laser beam profile for different heating laser powers P_{NIR} (Figure 3b). The CCD images of the blue laser spot at a fixed height (Z = 4 μm) for different values of P_{NIR} enable us to visually appreciate the induced Z-shift of the focus (insets of Figure 3b). For further quantification, we measure the vertical profile of the blue focal spot and find a Z-shift of 5 and 15 μm for P_{NIR} = 10 and 30 mW, respectively. This establishes the sensitivity of the focus shift to be 500 nm/mW, which corresponds to 230 nm/°C when using the temperature power calibration of Figure 2b. Thereafter, we record the focus shift as a function of laser power (Figure 3c) and observe a linear relationship. Next we quantify the lateral dimension of the region affected by an APT lens created by a 5 μm radius NR disk. To do so, we image through the APT lens a grating positioned on top of the water chamber. The ratio of the grating visibility with (P_{NIR} = 45 mW) and without (P_{NIR} = 0 mW) heating shows that the APT lens affects the focus over a region of about 13 μm (fwhm of curve Figure 3d). This value is close to the one obtained theoretically when considering a homogeneous gold disk of the same size and heated to about 70 °C (see Supporting Information, section 1).

To complete the characterization of the APT lens, we experimentally determine its rise time. The temperature was measured above NR disks of different radii while turning on and off the heating laser (Figure 4). The time from when the laser is turned on until the temperature reaches its steady state corresponds to the rise time of the lens. The temperature was measured using the same FPA method as referred to above (see Figure 2). In general, the time response is determined by the size of the heating source and the thermal diffusivity of the environment.[30] The characteristic time of a thermal process can be theoretically estimated by applying dimensional analysis to the heat transport equation and is given by[27,30,34]

$$t_T = L^2/\alpha$$

where t_T is the characteristic time for temperature establishment, L is the characteristic size of the system, and α is the thermal diffusivity of the media.

DOI: 10.1021/ph500392c
ACS Photonics 2015, 2, 355−360

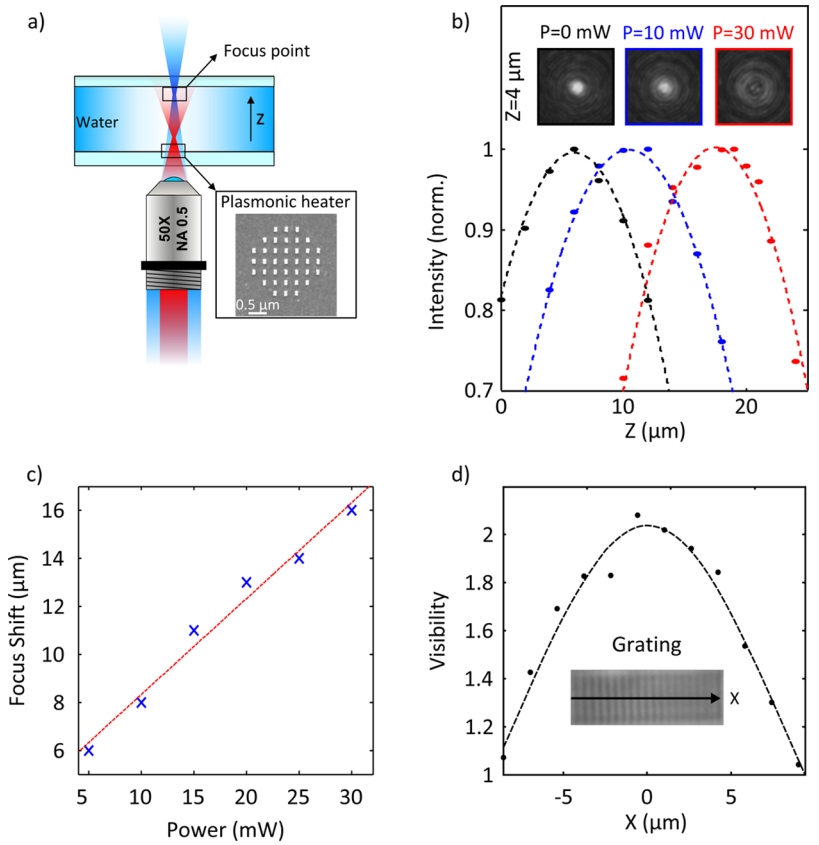

Figure 3. Experimental characterization of the APT lens. (a) Sketch of the experimental set up. The plasmonic structures are sealed in a closed chamber filled with water and heated with a 800 nm laser focused with a 50× microscope objective (NA = 0.5). The focus of the 800 nm laser is set to shed light on the whole 5 μm radius gold NR disk. (b) Intensity Z-profile of a focused 473 blue laser beam imaged on a CCD for three different powers of the 800 nm heating laser (black, 0 mW; blue, 10 mW; red, 30 mW). When using a power of 30 mW the blue focal point is shifted by a little more than 10 μm. The top insets correspond to the CCD image of the blue laser beam at a fixed height (Z = 4 μm) for the different incoming powers of the 800 nm laser. (c) Focus shift as a function of the 800 nm laser power shined on the thermal lens. (d) Visibility profile along the X-axis of a 2.5 μm pitch grating. The 5 μm APT lens (located at the bottom of the water chamber) is positioned at the center of the grating (placed above the water chamber). Each data point of the graph corresponds to the grating visibility ratio with (P_{NIR} = 45 mW) and without (P_{NIR} = 0 mW) thermal lensing. For visual appreciation, see video S4 in Supporting Information, where the power of the lens is changed both gradually and in discrete steps.

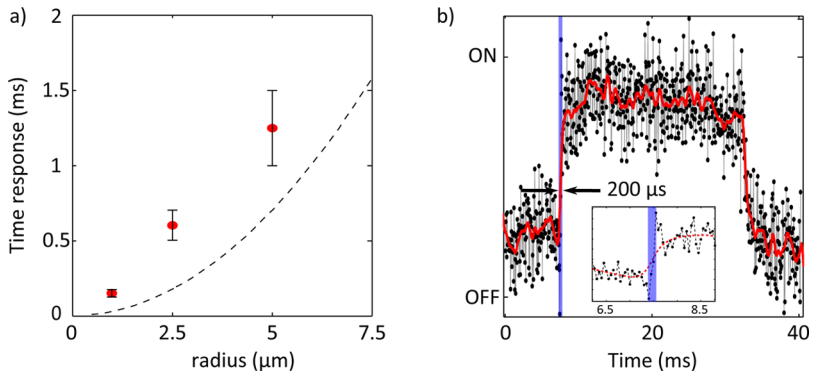

Figure 4. Time response of the APT lens. (a) Time response of the APT lens as a function of the size of the NR disk radius. The red dots show experimental results, and the black dashed line corresponds to the dimensional analysis equation described in the main text for $\alpha_{water} \approx 1.43 \times 10^{-6}$ m^2/s. (b) Experimental data showing the subms rise time of an APT lens made of a 1 μm radius gold NR disk. A zoomed view of the activation area can be seen in the inset. The measurement points were collected with a time resolution of 50 μs.

Data acquired on gold NR discs of 5, 2.5, and 1 μm radii give rise times of 1.5, 0.6, and 0.2 ms, respectively (Figure 4). This experiment confirms the decrease in time response for decreasing NR disk radius and shows that the APT lens can be much faster than other existing reconfigurable microlenses for which the time response is generally greater than a few milliseconds.[10−13,15,16,21]

Finally, we aim at demonstrating the applicability of the APT lens as an adaptive optical element for microscopy. Using the optically induced heat generation, it is possible to vary not only

DOI: 10.1021/ph500392c
ACS Photonics 2015, 2, 355−360

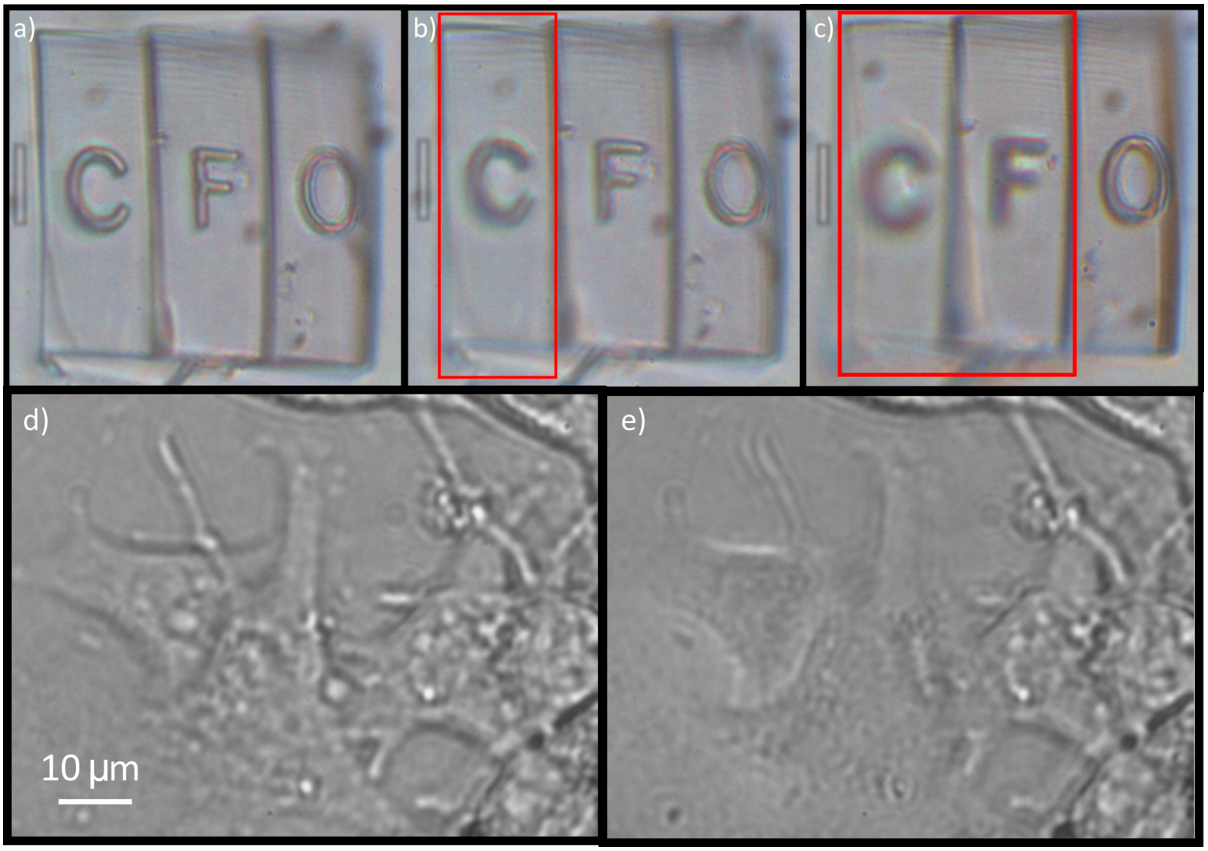

Figure 5. Application of the APT lens to microscopy and adaptive optics. (a) Bright field imaging of a sample composed of different letters located on different *Z*-planes separated by 5 μm steps (the scale bar on the left side corresponds to 50 μm). The picture, recorded without activating the APT lens, is originally focused on the "C" letter. (b, c) APT lens is locally activated in different regions of the field of view, indicated by a red box, which results in a controllable local defocusing. (d, e) APT lens tuning enables to inspect different planes of the B16−F10 cells. The full video showing the reconfigurable imaging for the biosample is available in the Supporting Information, S5.

the focal distance of the whole lens but also to easily and dynamically select the location of the lensing area within the field of view. To illustrate this aspect, an APT lens made of a large array of gold nanorods (few hundred of micrometers) was fabricated and integrated into a thin water chamber as previously described. The NIR heating laser is moved to different regions of this array with the aid of a steering mirror. In this configuration, the size of the thermal lens and the heating area is defined by the size of the heating beam or, more generally, by the overlap between the heating beam and the plasmonic array. When combined with a galvanometric mirror, this configuration allows fast spatial reconfiguration of the image plane. Furthermore, creation of multiple lenses can be achieved by splitting the heating laser beam.

As a primary test we use a three-dimensional sample composed of different letters located on different *Z*-planes separated by 5 μm steps (the scale bar on the left side corresponds to 50 μm). In Figure 5a, the sample is initially focused on the "C" letter in the absence of the heating laser. Subsequently, we record the optical image for different positions and sizes of the NIR laser spot (P_{NIR} = 30 mW) indicated by a red square in Figure 5b,c. In the region where the APT lens is activated, the image focal plane is locally shifted, which results in a defocusing of the letters in that region. Indeed, while the contour of the letters "CFO" can be individually resolved in Figure 5a, they appear blurry in Figure 5b,c (letters "C" and "CF", respectively). In addition to this 3D artificial sample, we also show in Figure 5d,e another proof of concept experiment in which the APT lens is used to image a living cell. Live cells, of the cell line B16−F10, were grown on a transparent Petri dish and then placed in the microscope in the imaging plane. Increasing the NIR power on the APT lens in the left region of the B16−F10 cell enables us to explore different details of the cell morphology (see video S5 in Supporting Information). An additional imaging experiment was performed on randomly distributed PS beads of different micrometric sizes (1, 3, 5, and 8 μm) and is presented in video S6 in Supporting Information.

CONCLUSION

The APT lens combines accurate and fast focus control with very simple implementation on most optical devices. Additionally, a wide range of properties can be achieved by using different thermo-optical materials. Indeed, the APT lens is a very general concept that involves a reconfigurable heat landscape at the vicinity of a transparent thermo-optical material. The implementation presented here, consisting of a patterned plasmonic surface immersed in water, is one among others. Alternative implementations could combine other heat nanosources with different thermo-optical materials (liquid, solid, or gas). We therefore foresee it benefiting to optical engineering as a whole. Among potential applications, the APT lens could be used to individually control the focus of arrays of microlenses, specifically for parallel optical monitoring or beam steering. Another of the major foreseen applications is related

DOI: 10.1021/ph500392c
ACS Photonics 2015, 2, 355−360

to the last set of experiments presented here and the use of the APT lens as a continuous adaptive lens operating in transmission which could be applied for example to 3D imaging.

■ ASSOCIATED CONTENT

Supporting Information

The method used to describe a heated structure in thermal contact with a thermo-optical material, in the framework of the paraxial approximation of the thick lens, is provided. We also discuss the lens aberrations and the possibility to induce anisotropy. This material is available free of charge via the Internet at http://pubs.acs.org.

■ AUTHOR INFORMATION

Corresponding Author

*E-mail: romain.quidant@icfo.es.

Notes

The authors declare no competing financial interest.

■ ACKNOWLEDGMENTS

This work was partially supported by the European Community's Seventh Framework Program under Grant ERC-Plasmolight (No. 259196) and Fundació privada CELLEX. R.M. acknowledges support of Marie Curie and NEST programs.

■ REFERENCES

(1) Nishiwaki, S.; Nakamura, T.; Hiramoto, M.; Fujii, T.; Suzuki, M. Efficient colour splitters for high-pixel-density image sensors. *Nat. Photonics* **2013**, *7*, 248−254.
(2) Kamei, Y.; et al. Infrared laser-mediated gene induction in targeted single cells in vivo. *Nat. Methods* **2009**, *6*, 79−81.
(3) Kim, P.; et al. In vivo wide-area cellular imaging by side-view endomicroscopy. *Nat. Methods* **2010**, *7*, 303−305.
(4) Park, J.-H.; Hong, K.; Lee, B. Recent progress in three-dimensional information processing based on integral imaging. *Appl. Opt.* **2009**, *48*, H77−H94.
(5) Fattal, D.; Li, J.; Peng, Z.; Fiorentino, M.; Beausoleil, R. G. Flat dielectric grating reflectors with focusing abilities. *Nat. Photonics* **2010**, *4*, 466−470.
(6) Fiorentino, M., Fattal, D. A.Beausoleil, R. G. *Control of light wavefronts.*
(7) Savage, N. Adaptive optics. *Nat. Photonics* **2008**, *2*, 756−757.
(8) Adaptive optics kits, tabletop deformable mirrors and more. *Nat. Photonics* **2011**, *5*, 27.
(9) Bifano, T. Adaptive imaging: MEMS deformable mirrors. *Nat. Photonics* **2011**, *5*, 21−23.
(10) Dong, L.; Agarwal, A. K.; Beebe, D. J.; Jiang, H. Adaptive liquid microlenses activated by stimuli-responsive hydrogels. *Nature* **2006**, *442*, 551−554.
(11) Lopez, C. A.; Hirsa, A. H. Fast focusing using a pinned-contact oscillating liquid lens. *Nat. Photonics* **2008**, *2*, 610−613.
(12) Fei, P.; et al. Discretely tunable optofluidic compound microlenses. *Lab Chip* **2011**, *11*, 2835−2841.
(13) Krupenkin, T.; Yang, S.; Mach, P. Tunable liquid microlens. *Appl. Phys. Lett.* **2003**, *82*, 316.
(14) Kuiper, S.; Hendriks, B. H. W. Variable-focus liquid lens for miniature cameras. *Appl. Phys. Lett.* **2004**, *85*, 1128.
(15) Liebetraut, P.; Petsch, S.; Liebeskind, J.; Zappe, H. Elastomeric lenses with tunable astigmatism. *Light Sci. Appl.* **2013**, *2*, e98.
(16) Zhang, W.; Zappe, H.; Seifert, A. Wafer-scale fabricated thermo-pneumatically tunable microlenses. *Light Sci. Appl.* **2014**, *3*, e145.
(17) Kim, J.; Serpe, M. J.; Lyon, L. A. Hydrogel microparticles as dynamically tunable microlenses. *J. Am. Chem. Soc.* **2004**, *126*, 9512−9513.
(18) Dong, L.; Agarwal, A. K.; Beebe, D. J.; Jiang, H. Variable-focus liquid microlenses and microlens arrays actuated by thermoresponsive hydrogels. *Adv. Mater.* **2007**, *19*, 401−405.
(19) Commander, L. G.; Day, S. E.; Selviah, D. R. Variable focal length microlenses. *Opt. Commun.* **2000**, *177*, 157−170.
(20) Ren, H.; Wu, S.-T. Adaptive liquid crystal lens with large focal length tunability. *Opt. Express* **2006**, *14*, 11292−11298.
(21) Campbell, K.; Fainman, Y.; Groisman, A. Pneumatically actuated adaptive lenses with millisecond response time. *Appl. Phys. Lett.* **2007**, *91*, 171111.
(22) Love, G. D. Wave-front correction and production of Zernike mode with a liquid-crystal spatial light modulator. *Applied Optics* **1997**, *36*, 1517−1524.
(23) Prietro , P. M.; Fernández, E. J.; Manzanera, S.; Artal, P. Adaptive Optics with a programmable phase modulator. *Optics Express* **2004**, *12*, 4059.
(24) Boyer, D.; Tamarat, P.; Maali, A.; Lounis, B.; Orrit, M. Photothermal imaging of nanometer-sized metal particles among scatterers. *Science* **2002**, *297*, 1160−1163.
(25) Gaiduk, A.; Yorulmaz, M.; Ruijgrok, P. V.; Orrit, M. Room-temperature detection of a single molecule's absorption by photothermal contrast. *Science* **2010**, *330*, 353−356.
(26) Berciaud, S.; Cognet, L.; Poulin, P.; Weisman, R. B.; Lounis, B. Absorption spectroscopy of individual single-walled carbon nanotubes. *Nano Lett.* **2007**, *7*, 1203−1207.
(27) Baffou, G.; Quidant, R. Thermo-plasmonics: using metallic nanostructures as nano-sources of heat. *Laser Photonics Rev.* **2013**, *7*, 171−187.
(28) Baffou, G.; et al. Photoinduced heating of nanoparticle arrays. *ACS Nano* **2013**, *7*, 6478−6488.
(29) Govorov, A. O.; Richardson, H. H. Generating heat with metal nanoparticles. *Nano Today* **2007**, *2*, 30−38.
(30) Baffou, G.; Quidant, R.; García de Abajo, F. J. Nanoscale control of optical heating in complex plasmonic systems. *ACS Nano* **2010**, *4*, 709−716.
(31) Bashkatov, A. N.; Genina, E. A. Water refractive index in dependence on temperature and wavelength: a simple approximation. *SPIE* **2003**, *5068*, 393−395.
(32) Richardson, H. H.; Carlson, M. T.; Tandler, P. J.; Hernandez, P.; Govorov, A. O. Experimental and theoretical studies of light-to-heat conversion and collective heating effects in metal nanoparticle solutions. *Nano Lett.* **2009**, *9*, 1139−1146.
(33) Baffou, G.; Kreuzer, M. P.; Kulzer, F.; Quidant, R. Temperature mapping near plasmonic nanostructures using fluorescence polarization anisotropy. *Opt. Express* **2009**, *17*, 3291−3298.
(34) Donner, J. S.; Baffou, G.; McCloskey, D.; Quidant, R. Plasmon-assisted optofluidics. *ACS Nano* **2011**, *5*, 5457−5462.

DOI: 10.1021/ph500392c
ACS Photonics 2015, 2, 355−360